16th World Conference on Earthquake Engineering, 16WCEE 2017
Santiago Chile, January 9th to 13th 2017
Paper N° 4578
Registration Code: S-J1463344832

LARGE-SCALE TESTING OF FRP-STRENGTHENED RC-SMRF T-BEAMS WITH RECTANGULAR WEB OPENINGS

S. Anacleto-Lupianez[1], L. Herrera[2], V. Slowik[3], A. Lemnitzer[4]

[1] *Graduate Student Researcher, University of California, Irvine, USA, sanaclet@uci.edu*
[2] *Graduate Student Researcher, University of California, Irvine, USA, lherrera@uci.edu*
[3] *Professor, Hochschule für Technik, Wirtschaft und Kultur, HTWK, Leipzig, Germany, volker.slowik@htwk-leipzig.de*
[4] *Professor, University of California, Irvine, USA, alemnitz@uci.edu*

Abstract

The nonlinear cyclic response of reinforced concrete special moment-resisting frame (RC-SMRF) beams with rectangular web openings was investigated through a series of large-scale experimental studies. A comprehensive set of T-beams was subjected to reverse cyclic loading and tested to complete structural failure. This paper presents the experimental results of three identical specimens with rectangular web opening: one specimen without external reinforcement and two duplicates strengthened in shear with externally bonded fiber-reinforced polymer (EB-FRP) sheets in two different U-wrap schemes. The EB-FRP reinforcement was applied to undamaged specimens in order to study the increase in strength, ductility and energy dissipation with respect to the externally unstrengthened beam. Two types of FRP composites were used: carbon fiber FRP laminates were applied at the fixed-end of the beams, whereas glass fiber FRP laminates were wrapped around the opening sections. The externally unstrengthened beam failed in the opening region, reaching a maximum strength of 646kN, a maximum displacement ductility of 2.2 and an ultimate drift ratio of 5.4%, while the application of EB-FRP reinforcement transferred the hinging zone to the beam-column interface and provided a maximum increase in peak force of 21%, in displacement ductility of 97% and in normalized cumulative energy dissipation of 203% (at peak).

Keywords: openings, large-scale testing, fiber-reinforced polymer, reinforced concrete, moment resisting frame beams.

1. Introduction

The introduction of transverse web openings in floor beams is an economical solution to reduce the story height of multistory buildings by enabling the passage of utility services through the structure, thus avoiding low hanging ceilings. However, geometric discontinuities such as web openings may alter the overall structural behavior of the member as a result of the reduction in overall beam stiffness and stress concentration around the openings. Hence, consequences include premature cracking, excessive deflections, and/or brittle failures at the weakened opening region. Historically, beam openings have been consciously avoided in seismically active regions given the lack of guidance, knowledge and test data available in the literature. Exemplarily, the American Concrete Institute code [1] does not include explicit design procedures for RC beams with web openings and limits its mention of opening design to the commentary to section 11.1.1.1 (ACI Committee 426, Section 4.7), which discusses work by Lorentsen (1962) [2] and Nasser et al. (1967) [3]. Both researchers concluded that openings in beams should be avoided near inflection points and additional stirrups are necessary around both sides of the opening.

Although a significant number of experimental and analytical studies have been conducted for the past fifty years on reinforced concrete (RC) beams with web openings ([4], [5], [6], [7], [8] [9], [10], [11], [12], [13], [14], [15], [16], [17], [18]), current literature only covers the behavior of perforated RC beams subjected to monotonic loading, with varying opening sizes, shapes and locations, and simply-supported and continuous boundary conditions. Therefore, this paper presents an unprecedented study that provides experimental data of the cyclic response of reinforced concrete special moment-resisting frame (RC-SMRF) beams with transverse web openings collected from large-scale tests. These results are vital for the calibration of component deterioration models of this special type of beams for use in nonlinear earthquake response analysis of RC framed buildings.

The overall experimental program consisted of eight large-scale T-shaped beam specimens tested to complete structural failure under quasi-static cyclic deformation reversals. Four specimens were strengthened with externally bonded fiber-reinforced polymer (EB-FRP) composites to assess the performance improvement using various FRP schemes and heavily instrumented to obtain detailed response information, as well as to provide data for development and validation of analytical models.

This paper presents the results of three test specimens, labeled S1, S1A and S1B hereafter. These three beam specimens were identical in geometry and internal reinforcement. Specimen S1 was a regular RC-SMRF T-beam with a web opening but no external reinforcement. Beams S1A and S1B were strengthened in shear at their critical sections (fixed-end support and opening) using two different wrapping schemes of EB-FRP reinforcement. Two types of FRP composites were implemented for specimens S1A and S1B: unidirectional carbon fiber-reinforced polymer (CFRP) sheets placed in a U-wrap configuration around the fixed-end of the beams, and bonded glass fiber-reinforced polymer (GFRP) sheets around the opening sections. The external FRP reinforcement was applied to undamaged specimens in order to study the increase in strength, ductility and energy dissipation with respect to the corresponding externally unstrengthened specimen, beam S1. A dense sensor network allowed the assessment of the hysteretic beam response over a wide range of vertical displacement levels, the evaluation of the suitability of the strengthening schemes, and the failure progress over the range of all damaged states.

2. Experimental Program

2.1. Specimens' Geometry and Reinforcement

Due to symmetry of SMRF beams between columns, test specimens were constructed as cantilever beams. Specimens were scaled by 80% in all geometric dimensions and reinforcement, in order to use US standard rebar sizes.

Specimens S1, S1A, and S1B had a length of 4.0 m (158 inches) and identical cross-sectional geometry: 97.5 cm (38.4 in) in depth and 61 cm (24 in) in width. The top slab was constructed with a width of 158.5 cm (62.4 in) and a thickness of 12.2 cm (4.8 in). The rectangular web openings were 97.5 cm (38.4 in) in length and 36.6 cm (14.4 in) in depth, which roughly represents 38% of the overall beam depth. The opening was located at a distance of 146.3 cm (57.60 in) from the fixed-end. All three beams were anchored in a reaction block with dimensions of 2.74 m (108 in) by 1.47 m (58 in) by 1.91 m (75 in) that simulated the in-situ beam-column connection.

The internal reinforcement of specimens S1, S1A, and S1B was also identical, with longitudinal and transverse reinforcement ratios at the fixed-end region (i.e. section "A" in Fig. 1) of ρ_l=0.0156, ρ_t=0.0041, respectively, and ρ_l=0.0218, ρ_t=0.0041 at the opening region (i.e. section "B" in Fig. 1). The geometry and internal reinforcement details for specimens S1, S1A, and S1B are specified in Fig. 1 and follow the layout of the existing building. US rebar diameters for #3, #4, #7, #8, #9 correspond to dimensions of 9.53 mm (0.375 in), 12.70 mm (0.5 in), 22.23 mm (0.875 in), 25.40 mm (1.000 in), 28.65 mm (1.128 in), respectively.

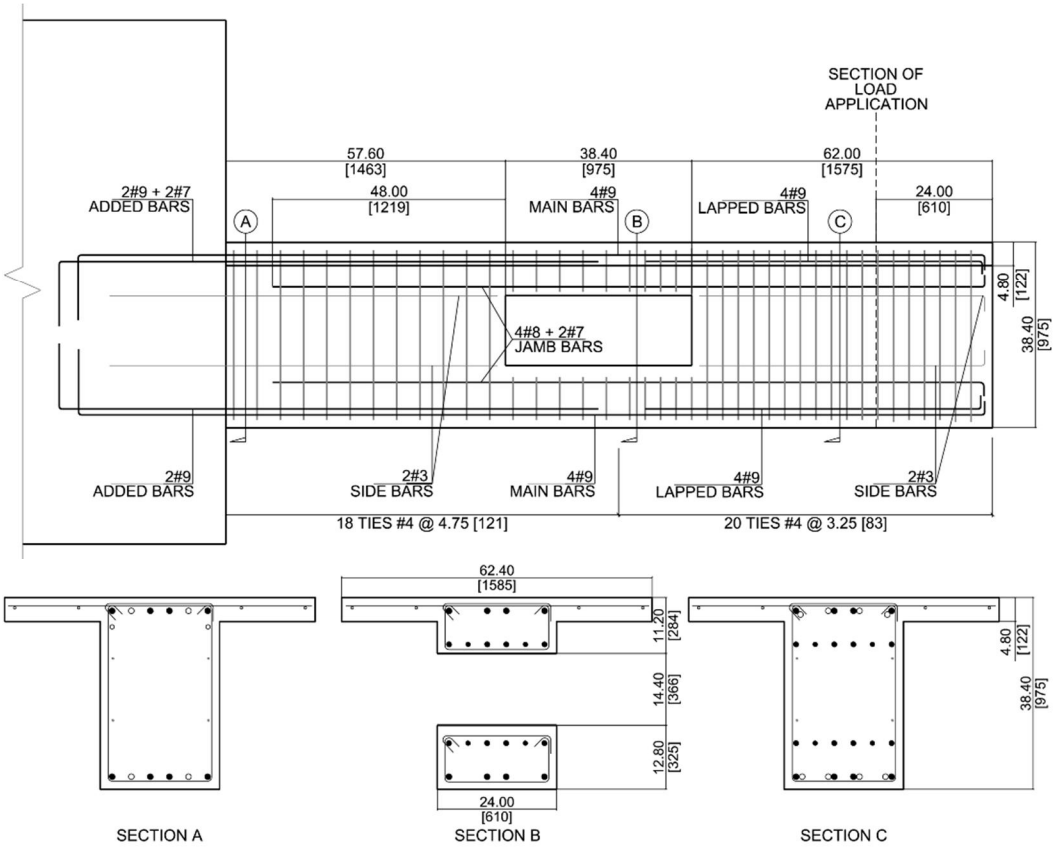

* Dimensions are in inches and [millimeters].

Fig. 1 – Geometry and internal reinforcement of specimens S1, S1A, and S1B.

Fig. 2 shows the details of the FRP shear-strengthening schemes used for beams S1A, and S1B. Two different FRP wrapping configurations were installed on beams S1A, and S1B, although the same materials were used for both specimens. In-situ CFRP was used at the fixed-end of the beams, whereas in-situ GFRP was applied around the opening region. Since the purpose of the installation of FRP wrap was to strengthen the specimens in shear, the unidirectional fibers of both CFRP and GFRP laminates were oriented vertically (i.e. perpendicular to the specimens' longitudinal axis).

For specimen S1A, one full-depth layer of CFRP was installed around the beam web, in a U-wrap configuration, at a distance of 5.1 cm (2 in) from the beam-column interface and with a strip width of 45.7 cm (18 in). An additional CFRP layer was installed on the soffit, extending 30.5 cm (12 in) on each side of the web. Two full-depth layers of GFRP U-wrap, 45.7 cm (18 in) wide, were installed on both sides of the opening. Two additional layers of GFRP were added on the soffit, only on the side of the opening close to the fixed support, and extending 20.3 cm (12 in) on each side of the web. The chord above the opening was also reinforced with two layers of GFRP in a U-wrap configuration. The bottom chord was fully wrapped with two layers of GFRP. All GFRP U-strips were anchored at the top with 12.7 cm (0.5 in) diameter anchors spaced 10.2 cm (4 in) and embedded into the slab 10.2 cm (4 in) at an angle of 60 degrees.

The configuration of the FRP shear-strengthening scheme of specimen S1B was similar to that of specimen S1A. The main difference at the fixed-end region was an additional CFRP U-strip under the slab that was anchored at the top using 12.7 cm (0.5 in) diameter anchors spaced 10.2 cm (4 in) and embedded into the slab 10.2 cm (4 in) at an angle of 60 degrees. At the opening region, only one full-depth layer of GFRP U-wrap was installed on both sides of the opening. Additionally, a 35.6 cm (14 in) long layer was installed under the slab. The top chord had an identical GFRP scheme as beam IA, consisting of two U-layers of GFRP anchored at the top. The bottom chord was fully wrapped with only one layer of GFRP. All GFRP U-strips were also anchored at the top with the same anchor type and spacing used in S1A.

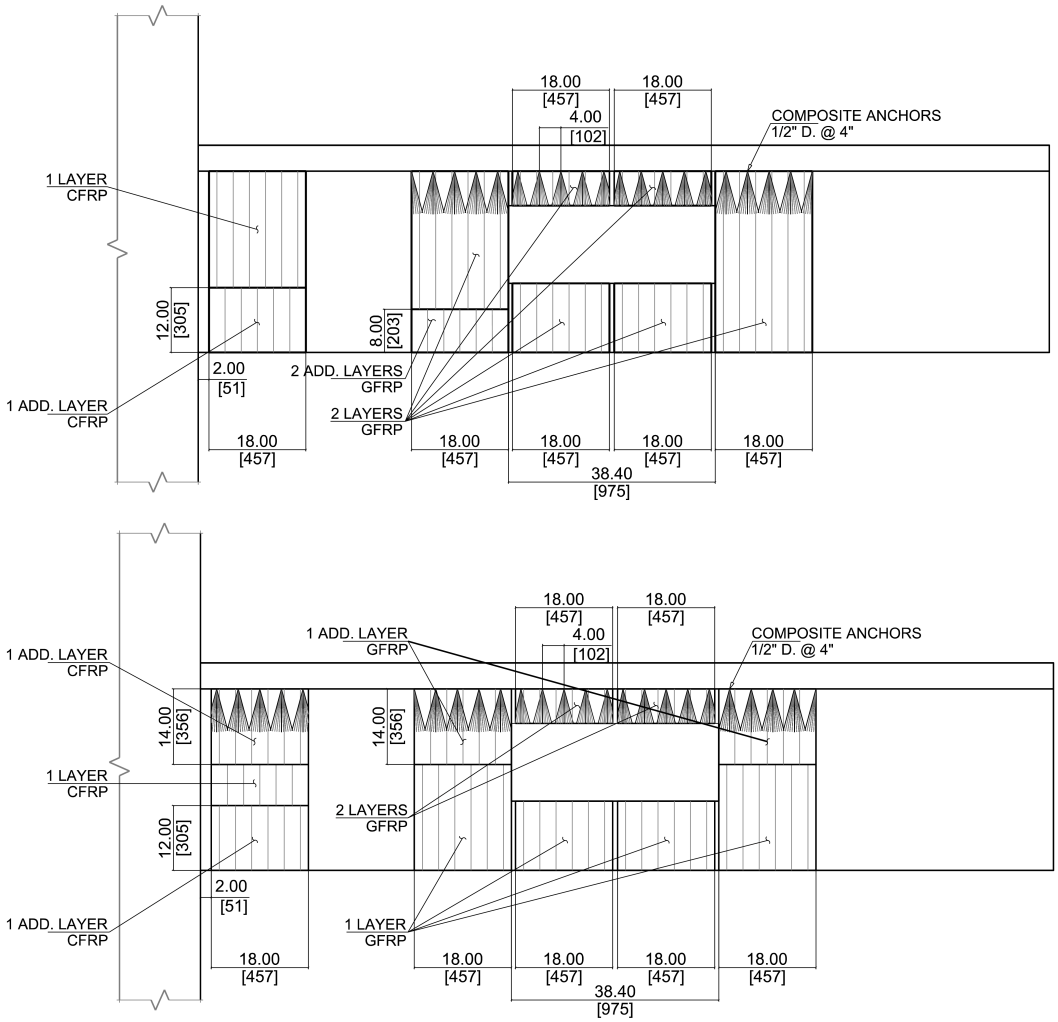

* Dimensions are in inches and [millimeters].

Fig. 2 – External FRP reinforcement of specimens S1A and S1B.

2.3. Material Properties

A concrete design mix with an average strength of 41.4 MPa (6 ksi) was selected to reach a target compressive strength of ≥ 7ksi at the day of testing. A commercially available design mixture with a maximum aggregate size of 3/8 in, a 3 in slump, and a sodium glucoheptonate based water reducer was utilized for all specimens. The average concrete compressive strength at test date for specimens S1, S1A, and S1B were, 53.2 MPa (7.72 ksi), 48.3 MPa (7.00 ksi) and 49.8 MPa (7.23 ksi), respectively. Reinforcing steel A615 grade 60 was used for the longitudinal reinforcement and A706 grade 60 for the transverse reinforcement of all specimens. The measured yield stress (f_y), ultimate stress (f_u) and percentage elongation at break for the #3, #7, #8, #9 longitudinal rebar and the #4 stirrups are summarized in Table 1.

Table 1 – Steel reinforcing bars mechanical properties.

Bar size	Diam.	Nominal f_y	Tested f_y	Tested f_u	Elong. in 8"
#	mm (in)	MPa (ksi)	MPa (ksi)	MPa (ksi)	%
3	9.53 (0.375)	414 (60)	485 (70.4)	764 (110.7)	13.0%
4	12.7 (0.50)	414 (60)	466 (67.6)	689 (100.0)	17.0%
7	22.22 (0.875)	415 (60)	445 (64.6)	734 (106.5)	15.0%
8	25.4 (1.000)	416 (60)	458 (66.4)	761 (110.4)	16.0%
9	28.65 (1.128)	417 (60)	462 (67.0)	739 (107.1)	18.0%

The composite gross mechanical properties, i.e., thickness (t), ultimate tensile strength (f_{fu}), ultimate tensile strain (ε_{fu}) and tensile modulus (E_f) in the fiber direction, for both the carbon fiber and glass fiber FRP composites installed on beams IA and IB are specified in Table 2.

Table 2 – FRP composites gross mechanical properties.

Fiber type	t	f_{fu}	ε_{fu}	E_f
-	mm (in)	MPa (ksi)	mm/mm	GPa (ksi)
carbon	1.0 (0.04)	986 (143)	0.010	95.8 (13.9x10^3)
glass	1.3 (0.05)	575 (83.4)	0.022	26.1 (3.79x10^3)

2.4. Moment and Shear Capacities

Table 3 presents analytically determined flexural capacities at yield (M_y) and ultimate points (M_u), as well as shear capacity, for specimens S1, S1A, and S1B in both loading directions and at the fixed-end section (i.e. section A) and the opening section (i.e. section B).

Moment-curvature (M-ϕ) relationships for sections A and B were obtained for measured material properties at the day of testing and using conventional reinforced concrete theory with the assumption that plane sections remain plane. The flexural capacity across the opening region, section B, was found to be similar to that of the solid section A, as chord members above and below the opening had greater depths than the ultimate compression stress blocks formed at M_u. Small divergences were attributed to differences in the reinforcement ratios in sections A and B. Since the fibers in the FRP laminates were oriented perpendicular to the beams axis, it is assumed that the FRP strengthening does not provide additional flexural capacity to specimens S1A and S1B. The calculated curvature values are conservative and represent flexural deformations under monotonic loading; thus, neither cyclic deterioration nor shear and bond slip deformations are accounted for. The M-ϕ analysis was performed using XTRACT v3.08.

The shear capacity (V_u) of all three specimens was calculated under the assumption that concrete does not contribute to the overall shear capacity (i.e. V_c = 0 kips) as flexural and flexural-shear cracks opened early during

the test at both top and bottom faces of the specimens. The steel contribution to the shear capacity (V_s) was computed per ACI 318-14 [1] Eq. (22.5.10.5.3) using measured material properties at the day of testing, and the additional FRP contribution to the shear capacities (V_f) of specimens S1A and S1B was computed according to the design guideline ACI 440.2R-08 [19]. The shear capacity at the opening section (i.e. section B) was calculated by adding the individual shear strength contributions of the top and bottom chord members.

Table 3 – Analytical moment and shear capacities of specimens I, IA and IB.

			BEAM I		BEAM IA		BEAM IB	
			down (+)	up (-)	down (+)	up (-)	down (+)	up (-)
SECTION A (fixed-end)	M_y	[kN-m]	1842	1487	1806	1458	1809	1460
	M_u	[kN-m]	2905	2404	2880	2384	2888	2391
	V_u @ V_c=0	[kN]	878	904	1066	1091	1074	1098
	V_f	[kN]	0	0	280	280	288	288
SECTION B (opening)	M_y	[kN-m]	1743	1672	1710	1640	1712	1642
	M_u	[kN-m]	2819	2904	2795	2879	2803	2887
	V_u @ V_c=0	[kN]	441	507	573	635	512	574
	V_f	[kN]	0	0	168	168	104	104

(1 kN = 0.225 kips; 1 kN-m = 0.738 kip-ft)

2.5. Test Procedure

The test specimens were subjected to reverse cyclic loading in the vertical direction to simulate the effects of earthquake-induced deformations. Loading was applied at 61 cm (24 in) from the free-end by means of a 1334 kN (300 kips) capacity hydraulic actuator and a U-shaped steel clamping system, as shown in Fig. 3. The clamp embraced the beam from the top and was connected with the specimen via six post-tensioned horizontal dywidag rods to facilitate an even, slip-free load distribution profile across the beam's depth. The reaction block was fastened to the strong floor and strong wall via post-tensioned dywidag bars, and additionally secured with two shear plates in the front to restrict any block rotation or sliding. Verification of zero block rotation and sliding was also monitored during load application and confirmed to be negligible.

Fig. 3 – Test setup.

Loading protocols were designed using ASCE 41-06, C2.8.1 recommendations to capture the anticipated failure mode, and consisted in stepwise increasing cyclic displacement reversals, with three cycles per each displacement level until reaching the Collapse Prevention (CP) structural performance level, and two cycles for levels beyond CP.

Table 4 – Load protocol details.

BEAM I	Drift	[%]	**0.0%**	**0.1%**	**0.4%**	**0.6%**	**0.9%**	**1.0%**	**1.5%**	**2.0%**	**3.0%**	**4.5%**	**5.4%**	
	Displ.	[cm]	0.1	0.4	1.4	2.1	3.1	3.5	5.1	6.9	10.3	15.4	18.4	
	Ductility	[cm/cm]	0.0	0.1	0.4	0.7	1.0	1.1	1.7	2.2	3.3	5.0	5.9	
	Load down	[kN]	53.5	144.7	322.7	428.9	565.3	568.0	615.5	646.2	521.6	274.0	155.2	
	Load up	[kN]	-54.4	-137.6	-284.6	-423.9	-544.4	-537.9	-564.5	-589.3	-478.9	-322.5	-230.1	
	Cycles	[No.]	2	3	3	3	3	3	3	3	2	2	1	
BEAM IA	Drift	[%]	**0.1%**	**0.2%**	**0.3%**	**0.4%**	**0.6%**	**0.8%**	**1.0%**	**1.5%**	**2.0%**	**3.0%**	**4.0%**	**6.0%**
	Displ.	[cm]	0.4	0.7	1.0	1.3	2.0	2.6	3.4	5.2	6.8	10.2	13.7	20.5
	Ductility	[cm/cm]	0.1	0.3	0.4	0.5	0.8	1.0	1.3	2.0	2.6	4.0	5.3	7.9
	Load down	[kN]	110.7	211.1	294.5	364.4	470.4	567.6	606.5	653.6	681.9	722.4	697.9	391.9
	Load up	[kN]	-92.1	-181.8	-272.0	-353.6	-467.6	-557.8	-574.2	-621.5	-656.3	-711.1	-694.6	-544.7
	Cycles	[No.]	3	3	3	3	3	3	3	3	3	3	3	2
BEAM IB	Drift	[%]	**0.1%**	**0.2%**	**0.4%**	**0.6%**	**0.8%**	**1.1%**	**1.6%**	**2.3%**	**3.3%**	**4.5%**	**6.0%**	
	Displ.	[cm]	0.3	0.7	1.3	2.0	2.6	3.8	5.5	7.8	11.3	15.3	20.4	
	Ductility	[cm/cm]	0.1	0.2	0.4	0.6	0.9	1.2	1.8	2.6	3.7	5.0	6.7	
	Load down	[kN]	133.6	202.2	321.7	447.8	540.8	616.6	667.8	713.3	748.9	561.6	400.3	
	Load up	[kN]	-177.5	-237.0	-368.7	-477.0	-551.6	-571.1	-624.0	-669.1	-715.1	-631.1	-552.0	
	Cycles	[No.]	3	3	3	3	3	3	3	3	3	2	2	

(1 cm = 0.394 inch; 1 kN = 0.225 kips)

2.6. Instrumentation

A total of 70, 68 and 64 sensors were installed on the test specimens S1, S1A, and S1B, respectively, in order to monitor beam displacements, rotations and internal strains during testing. Specifically, a total of 28 LVDT's were installed on each beam; 14 of them were mounted on one side of the beams web in a longitudinal configuration to measure flexural deformations, and the remaining 14 were mounted on the opposite side in a X configuration to measure shear deformations. Six string potentiometers were installed on the beams' soffit and attached to the strong floor to assess the beams deflection curves. Two additional string potentiometers were installed on the reaction block ends in order to monitor its displacement and rotation, which were found to be negligible. Strains in the reinforcing steel were monitored using a total of 36, 28 and 28 strain gauges in specimens S1, S1A, and S1B, respectively. Instrumented reinforcing bars included the main longitudinal reinforcement (top and bottom), the stirrups closer to the opening corners and the stirrup in the middle of the opening section. The strains in the GFRP installed around the opening were also monitored in specimen IA via 4 additional strain gauges, 2 on each side of the opening, and installed directly on the surface of the composite laminates. Fig. 4 shows photographs of the external sensors described above.

Fig. 4 – External instrumentation for specimen I.

3. Test Results and Discussions

3.1. Crack Patterns and Failure Modes

3.1.1. Specimen S1 (no FRP)

Fig. 5 depicts the crack patterns of specimen I at complete structural failure. Initial, vertical, flexure-type cracks at the support and opening regions occurred at a drift ratio of 0.12% approximately *h/2* from the beam-column interface (where *h* is the overall beam height). Cracking in the opening region started at both the opening corners and the chord members. Long diagonal tension cracks were initiated at 0.63% drift ratio along the beam segment comprised between the tip and the opening. Vertical flexural cracks along the chord members progressively turned into deeper and inclined flexure-shear cracks. As shown in photographs of Fig. 6, bond splitting cracks developed in a later loading stage along the jamb bars and main reinforcement of the bottom chord. Spalling of the cover concrete occurred first at the top chord. Extensive crushing and spalling of the confined concrete occurred at both top and bottom chord members at drift level of 4.5% and lead to collapse. Cracking patterns suggest that the top chord failed primarily by the formation of diagonal cracks in both directions (shear failure), while the bottom chord displayed a predominantly bond splitting failure mode. This type of failure was likely due to inadequate detailing provided around the opening, with neither added nor lapped reinforcing bars being continuously developed along the whole span of the chord members, thus creating an abrupt discontinuity of the longitudinal reinforcement close to the opening mid-section.

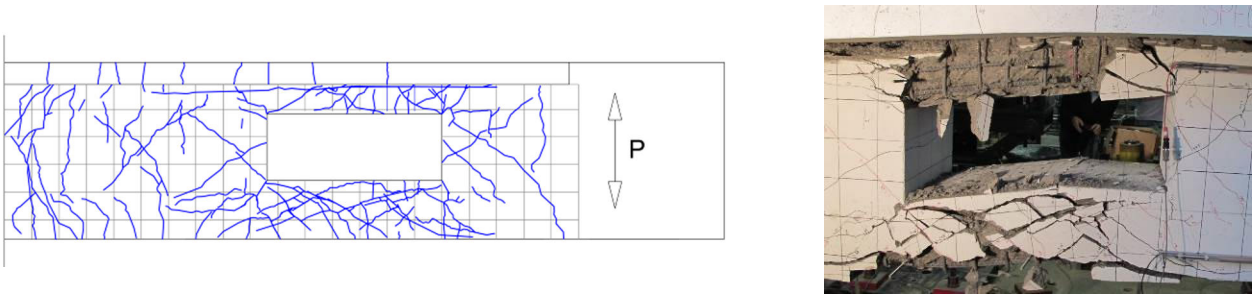

Fig. 5a & b: – Crack patterns in specimen S1 at drift ratio 4.5% (a, left) and photograph of opening region cracks and damage at drift ratio 4.5% (b, right)

3.1.2. Specimens IA & IB (FRP-strengthened)

For specimens S1A and S1B, crack patterns were only visible in the area between the CFRP and the GFRP laminates. CFRP, which wrapped the fixed-end region, was painted white for easier monitoring of cracks at the hinging region.

Specimen S1A: The first observed cracks in the concrete were vertical flexural cracks originating from the tension top face of the beam and appeared while loading in the downward direction at 0.19% drift ratio. A long diagonal tension crack developed simultaneously across the painted concrete region. First visible vertical cracks along the CFRP, originating from the top face occurred at 0.57% drift and continued through higher drift levels. No discernable cracks were observed in the opening region, attributed to the presence of the GFRP wrap. Widening of the cracks and crushing of the concrete at the hinging region, next to the support, eventually lead to vertical tearing of the CFRP laminate at 3.0% drift, as shown in Fig. 6a&b. Spalling of the cover concrete commenced at the same drift level at the portion of the slab next to the beam-column interface. At 4.0% drift, delamination of the CFRP progressed and the wrap ruptured along the soffit of the beam, resulting into concrete detachment previously prevented by the CFRP. Almost all of the bottom longitudinal reinforcement became visible. At the top part of the member, large pieces of concrete disintegrated but were contained by the transverse reinforcement.

Specimen S1B: Cracking initiated during the first downward cycle at 0.38% drift in both the concrete and the CFRP. Flexural cracks developed from the tension face and progressively turned into long shear diagonal cracks. During subsequent drift levels (i.e. 0.57% and 0.75%), new vertical cracks appeared along the lateral faces of the

CFRP wrap, at the same time as new flexural-shear cracks developed in the visible concrete section. Similar to Specimen S1A, Specimen S1B showed no apparent damage or severe cracking at the opening region throughout the entire test. At 2.30% drift, vertical cracks on the CFRP laminates widened substantially; complete detachment occurred at 3.3% drift. At 4.5% drift, an approximately 7.62 cm (3 in) wide strip of CFRP detached all the way around the opening (Fig. 6c), including the intact composite anchors, which resulted in significant concrete spalling from the soffit of the beam. Specimen IB failed at the plastic hinge developed next to the fixed-end of the beam, similar to Specimen IA.

Fig. 6a, b &c – Crack patterns in specimen IA at failure region (i.e. fixed-end) at 3.0% and 4.0% drift (a & b, left & middle), and crack patterns in specimen IB at failure region (i.e. fixed-end) at 4.5% drift (c, right).

3.2. Hysteretic response

Test results for specimens S1, S1A, and S1B are summarized in Table 5 and Figs. 7 & 8. The flexural cracking strength ($F_{cr,f}$) and the diagonal tension cracking strength ($F_{cr,s}$) were both estimated based on visual observations during the test, and correspond to the load steps at which the first flexure and diagonal cracks were detected. The yield strength (F_y), yield displacement (Δ_y) and yield drift ratio (δ_y) correspond to the point of the cyclic envelope curve at which the first substantial change of stiffness is observed, whereas the peak strength (F_p), peak displacement (Δ_p) and peak drift ratio (δ_p) correspond to the point of peak strength. The ratio of the peak deformation divided by the yield deformation represents the displacement ductility capacity (μ) of the member.

Table 5 – Summary of experimental hysteretic results.

	BEAM I		BEAM IA		BEAM IB	
	down (+)	up (-)	down (+)	up (-)	down (+)	up (-)
$F_{cr,f}$ [kN]	144.7	137.6	211.1	181.8	321.7	368.7
$F_{cr,s}$ [kN]	428.9	423.9	211.1	353.6	321.7	368.7
F_y [kN]	565.3	544.4	567.6	557.8	595.9	551.6
Δ_y [cm]	3.1	3.0	2.6	2.6	3.0	2.6
δ_y [%]	0.91%	0.89%	0.76%	0.75%	0.89%	0.75%
F_p [kN]	646.2	589.3	722.4	711.1	748.9	715.1
Δ_p [cm]	6.9	6.8	10.2	10.2	11.3	11.4
δ_p [%]	2.03%	2.01%	3.01%	3.01%	3.31%	3.35%
$\mu=\Delta_p/\Delta_y$ [cm/cm]	2.2	2.3	4.0	4.0	3.7	4.4

(1 cm = 0.394 inch; 1 kN = 0.225 kips; 1 kN-m = 0.738 kip-ft)

Vertical load-displacement relationships are presented in Figs. 7. Positive displacement values correspond to the downward loading direction (i.e. slab in tension), while negative values correspond to upward loading (i.e. slab in compression). The performance of the FRP-strengthened specimens S1A and S1B is compared to that of the unstrengthened specimen, S1. Test results indicate that considerable enhancement of the ultimate strength, the ductility and the energy dissipation capacity was achieved by means of both FRP-strengthening schemes. The

minimum and maximum increase in peak strength attained with the FRP reinforcement with respect to the unstrengthened specimen (i.e. S1) were 12% and 21%, respectively, and the range of increase in terms of ductility was 66% to 97%. In general, both wrapping schemes performed similarly, with the higher peak loads and displacements reached by S1B being mainly attributed to the higher drift applied on the beam (3.3% drift for S1B vs. the 3% drift for S1A).

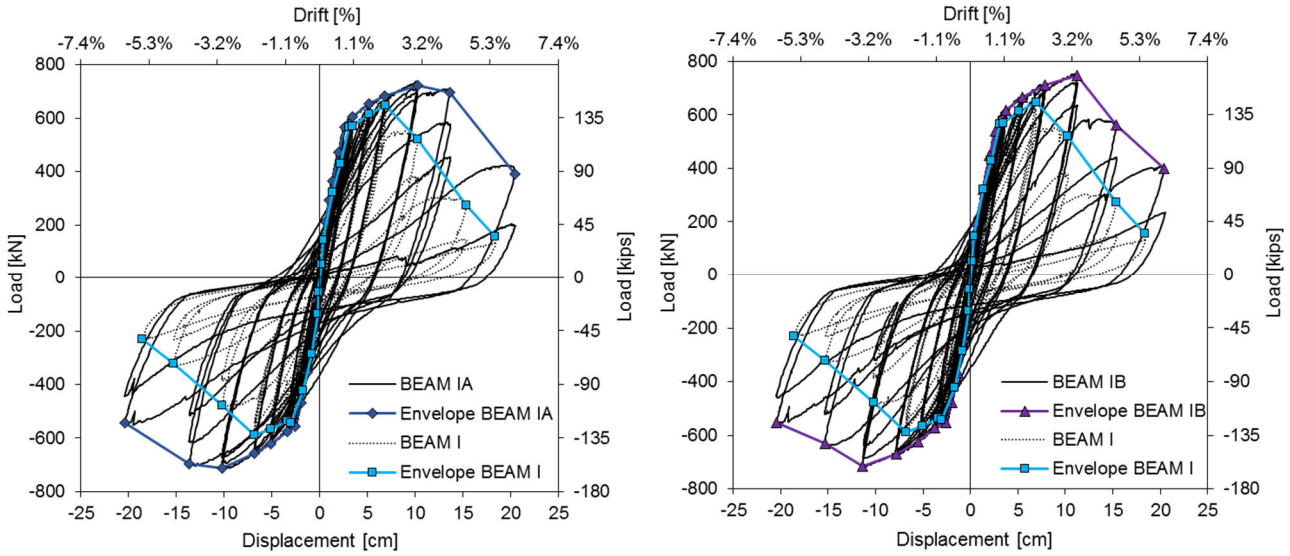

Fig. 7 – Vertical load versus tip displacement.

The history of (cumulative) normalized hysteretic energy (NHE) dissipation for the discussed three specimens is presented in Fig. 8 with respect to the applied drift levels. NHE at a given cycle was computed as the summation of the dissipated hysteretic energies (HE) of the current and preceding cycles normalized by twice the elastic strain energy, where each HE was obtained as the enclosed area of the corresponding load-deformation hysteretic loop. The NHE at yield for specimens S1, S1A and S1B was 1.0, 1.0, and 0.9, respectively, and the corresponding NHE dissipated at peak capacity accumulated to 8.5, 23.8, and 25.9, which represents an increase of 178% for S1A and 203% for S1B with respect to specimen S1. Specimen S1 showed a much flatter increase rate of NHE than S1A and S1B associated with much more severe cyclic degradation than the FRP-strengthened specimens, which manifested in the form of intense pinching of the loops and dramatic strength loss after peak.

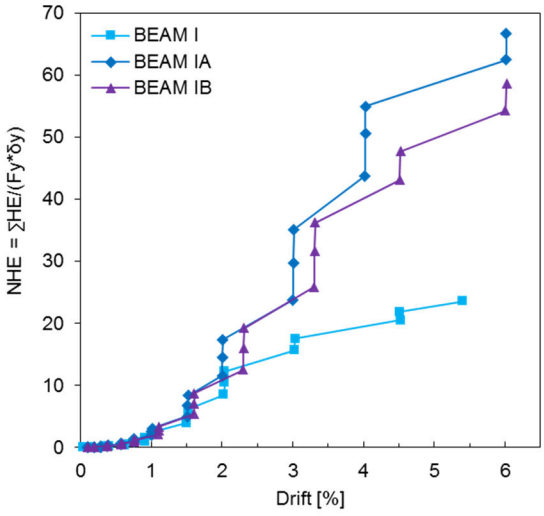

Fig. 8 – History of (cumulative) normalized hysteretic energy (NHE) dissipation.

4. Conclusions

Three identical large-scale T-beam specimens, part of moment resisting frame beams in an existing building, were subjected to reverse cyclic loading to evaluate the effectiveness of external FRP strengthening at the beam-column connection and the beam opening region. The externally unstrengthened specimen, S1, showed early cracking in the opening region simultaneously with cracks in the fixed-end region. Shear-type failure occurred at the opening region and is mainly attributed to the discontinuity of the added and lapped rebar along the chord members. The two FRP-strengthened specimens showed an overall satisfying performance by preventing failure at the opening and successfully relocating the plastic hinge to the beam-column interface. Simultaneously, an increase in peak strength (up to 21%), ductility capacity (up to 97%) and energy dissipation (up to 203% at peak) compared to their unstrengthened counterpart was observed. Although flexure deformations were prevailing, all specimens exhibited extensive diagonal cracking, which suggested an important contribution of shear in their behavior. This behavior will be investigated in detail in future publications. All three specimens, including the externally unstrengthened beam (i.e. specimen S1), performed with adequate ductility, i.e., crushing of concrete occurred after the formation of the failure mechanism at the critical section only. The FRP-strengthening schemes of specimens S1A and S1B exhibited comparable performance. Thus, since the amount of external FRP reinforcement used on specimen S1B was reduced with respect to that installed on S1A, the former is likely to be preferred for the strengthening of the existing beam condition.

5. Acknowledgements

The authors would like to acknowledge the entire Project team, specifically Dr. Winston Chai and Mr. Todd Erickson who significantly contributed in executing the experimental program. We would also like to acknowledge The UCI Structural Laboratory manager, Dr. Sergio Carnalla and all undergraduate and graduate students that helped during test setup, instrumentation and execution.

6. References

[1] ACI Committe 318 (2014): Building code requirements for structural concrete (ACI 318-14) and commentary. *American Concrete Institute*.

[2] M. Lorentsen (1962): Holes in reinforced concrete girders. *BYGGMASTAREN*, Vol. 41, No. 7, July, 141-152 Transl. from Swedish by PCA, Chicago, Illinois.

[3] K. W. Nasser, A. Acavalos, and H. R. Daniel (1967): Behavior and Design of Large Openings in Reinforced Concrete Beams. *ACI J. Proc.*, vol. 64, no. 1, pp. 25–33.

[4] J. M. Hanson (1969): Square openings in webs of continuous joists. *Portland Cement Association R D Lab Bull*.

[5] N. F. Somes and W. G. Corley (1974): Circular openings in webs of continuous beams. *Spec. Publ.*, vol. 42, pp. 359–398.

[6] G. B. Barney, P. C. Association, and others (1978): Behavior and design of prestressed concrete beams with large web openings. *Portland Cement Association*.

[7] M. A. Mansur, K. H. Tan, and S. Lee (1984): Collapse loads of R/C beams with large openings. *J. Struct. Eng.*, vol. 110, pp. 2602–2618.

[8] M. A. Mansur, K. H. Tan, and S. L. Lee (1985): Design method for reinforced concrete beams with large openings. *Journal Proceedings*, vol. 82, no. 4, pp. 517–524.

[9] M. A. Mansur (1988): Ultimate strength design of beams with large openings. *Int. J. Struct.*, vol. 8, no. 2, pp. 107–125.

[10] W. B. Siao and S. F. Yap (1990): Ultimate behaviour of unstrengthen large openings made in

existing concrete beams. *J. Inst. Eng.*, vol. 30, no. 3, pp. 51–57.

[11] M. A. Mansur, Y. F. Lee, K. H. Tan, and S. L. Lee (1991): Tests on RC continuous beams with openings. *J. Struct. Eng.*, vol. 117, no. 6, pp. 1593–1606.

[12] M. A. Mansur (1992): Deflections of reinforced concrete beams with web openings. *ACI Struct. J.*, vol. 89, no. 4, pp. 391–397.

[13] K.-H. Tan and M. A. Mansur (1996.): Design procedure for reinforced concrete beams with large web openings. *ACI Struct. J.*, vol. 93, no. 4, pp. 404–411.

[14] K.-H. Tan, M. A. Mansur, and L.-M. Huang (1996): Reinforced concrete T-beams with large web openings in positive and negative moment regions. *ACI Struct. J.*, vol. 93, no. 3, pp. 277–289.

[15] M. A. Mansur (1998): Effect of openings on the behaviour and strength of R/C beams in shear. *Cem. Concr. Compos.*, vol. 20, no. 6, pp. 477–486.

[16] K.-H. Yang, H.-C. Eun, and H.-S. Chung (2006): The influence of web openings on the structural behavior of reinforced high-strength concrete deep beams. *Eng. Struct.*, vol. 28, no. 13, pp. 1825–1834.

[17] K.-H. Yang and A. F. Ashour (2008): Effectiveness of web reinforcement around openings in continuous concrete deep beams. *ACI Struct. J.*, vol. 105, no. 4, p. 414.

[18] T. El-Maaddawy and B. El-Ariss (2012): Behavior of concrete beams with short shear span and web opening strengthened in shear with CFRP composites. *J. Compos. Constr.*, vol. 16, no. 1, pp. 47–59.

[19] ACI Committe 440 (2008): Guide for the design and construction of externally bonded FRP systems for strengthening concrete structures (ACI 440. 2R-08). *American Concrete Institute*. Farmington Hills, MI..